Journal of Experimental Botany, Vol. 73, No. 1 pp. 263–274, 2022
https://doi.org/10.1093/jxb/erab427 Advance Access Publication 27 September 2021

RESEARCH PAPER

Ammonium nutrition interacts with iron homeostasis in *Brachypodium distachyon*

Marlon De la Peña[1], Agustín Javier Marín-Peña[1], Leyre Urmeneta[1], Inmaculada Coleto[1], Jorge Castillo-González[2], Sebastiaan M. van Liempd[3], Juan M. Falcón-Pérez[3,4,5], Ana Álvarez-Fernández[2], María Begoña González-Moro[1] and Daniel Marino[1,5,*]

[1] Department of Plant Biology and Ecology, University of the Basque Country (UPV/EHU), E-48940, Leioa, Spain
[2] Department of Plant Nutrition, Aula Dei Experimental Station, Consejo Superior de Investigaciones Científicas (EEAD-CSIC), E-50059, Zaragoza, Spain
[3] Metabolomics Platform, CIC bioGUNE-BRTA, Derio, Spain
[4] Centro de Investigación Biomédica en Red de enfermedades hepáticas y digestivas (CIBERehd), Madrid, Spain
[5] Ikerbasque, Basque Foundation for Science, E-48011 Bilbao, Spain

* Correspondence: daniel.marino@ehu.eus

Received 14 July 2021; Editorial decision 15 September 2021; Accepted 16 September 2021

Editor: Stanislav Kopriva, University of Cologne, Germany

Abstract

Most plant species develop stress symptoms when exposed to high ammonium (NH_4^+) concentrations. The root is the first organ in contact with high NH_4^+ and therefore the first barrier to cope with ammonium stress. In this work, we focused on root adaptation to ammonium nutrition in the model plant *Brachypodium distachyon*. Proteome analysis revealed changes associated with primary metabolism, cell wall remodelling, and redox homeostasis. In addition, it showed a strong induction of proteins related to methionine (Met) metabolism and phytosiderophore (PS) synthesis in ammonium-fed plants. In agreement with this, we show how ammonium nutrition impacts Met/*S*-adenosyl-Met and PS metabolic pathways together with increasing root iron content. Nevertheless, ammonium-fed plants displayed higher sensitivity to iron deficiency, suggesting that ammonium nutrition triggers impaired iron utilization and root to shoot transport, which entailed an induction in iron-related responses. Overall, this work demonstrates the importance of iron homeostasis during ammonium nutrition and paves a new way to better understand and improve ammonium use efficiency and tolerance.

Keywords: Ammonium, *Brachypodium*, iron, metabolism, methionine, nitrate, nitrogen, phytosiderophores, root.

Introduction

Plants take up nitrogen (N) from the soil mostly in the form of nitrate (NO_3^-) and ammonium (NH_4^+). Regardless of the N source, N assimilation into biomolecules occurs from NH_4^+ incorporation into carbon (C) skeletons, and thus the direct uptake of NH_4^+ bypasses the energy-consuming NO_3^- reduction process (Marschner, 2012). Importantly, ammonium-based

nutrition in combination with nitrification inhibitors has been shown to lower the negative impact N fertilization has on the environment (Beeckman *et al.*, 2018; Huérfano *et al.*, 2018).

Apart from N, plants need 16 other essential nutrients to complete their life cycle. Genetic, physiological, and biochemical interactions among elements have been reported (Bouain *et al.*, 2019). In particular, the N source is known to interact with the acquisition and homeostasis of other macro- and micronutrients. For instance, it has been extensively reported that plants grown under NH_4^+ supply display a lower content of cations such as potassium (K^+), calcium (Ca^{2+}), and magnesium (Mg^{2+}) with respect to nitrate nutrition because of their direct competition with the uptake of NH_4^+ (Van Beusichem *et al.*, 1988; Roosta and Schjoerring, 2007). In addition, molecular players that connect NO_3^- signalling to phosphorus (P) deficiency have been identified, such as the NO_3^- transporter NPF7.3/NRT1.5 (Cui *et al.*, 2019) or the transcription factor HRS1 (hypersensitive to low Pi-elicited primary root shortening) (Medici *et al.*, 2015). NH_4^+ also appears to promote P remobilization of the cell wall (Zhu *et al.*, 2016). Moreover, the N source interacts with sulfur (S). For instance, ammonium nutrition enhances sulfate assimilation and uptake (Van Beusichem *et al.*, 1988; Gerendás *et al.*, 1997; Coleto *et al.*, 2017). Although less attention has been paid to the interactions of micronutrients with the N source, recent works have provided support for the interaction between NH_4^+ and iron (Fe) homeostasis in rice (Zhu *et al.*, 2018) and Arabidopsis (Zhu *et al.*, 2019; Coleto *et al.*, 2021). Among others, NH_4^+ supply was reported to promote Fe release from the cell wall probably through the stimulation of nitric oxide synthesis (Zhu *et al.*, 2018, 2019).

When NH_4^+ is present at high concentrations in the soil, it provokes a marked stress to most plant species, and interactions with other nutrients appear essential for plants to deal with ammonium stress. For instance, the concentration of K^+ in the medium has been extensively shown to be associated with ammonium stress symptoms (Balkos *et al.*, 2010; Coskun *et al.*, 2014). In addition, the increase of Fe supply also improved *Arabidopsis thaliana* growth under ammonium nutrition (Coleto *et al.*, 2021).

Fe is an important determinant in building prosthetic groups of proteins such as Fe–S clusters and haem groups, which means that Fe participates in many essential plant functions (e.g. chlorophyll synthesis and electron transfer between PSI and PSII). Thus, any defect in Fe availability has a great impact on plant growth and quality. Fe is often present in insoluble complexes with low bioavailability, particularly in calcareous/alkaline soils (Briat *et al.*, 2015). To face this limitation, plants have developed two strategies to solubilize Fe in the rhizosphere. Most flowering plants display the so-called strategy I or reduction-based strategy. However, graminaceous species, display strategy II or the chelation-based strategy. Exceptionally, rice has acquired a combined strategy (Ricachenevsky and Sperotto, 2014). Strategy I is a three-step process that starts with proton release from the roots to increase local Fe^{3+} solubility. Then, Fe^{3+} is reduced to Fe^{2+} by a plasma membrane-bound ferric reductase. Finally, Fe^{2+} is taken up by the root via IRTs (iron-regulated transporters). In strategy II, graminaceous plants synthesize compounds of the mugineic acid (MA) family called phytosiderophores (PSs) that are released into the rhizosphere via TOM1 (transporter of mugineic acid family phytosiderophores 1). PSs bind Fe^{3+}, forming Fe^{3+}–PS complexes that enter into root cells by Yellow Stripe/Yellow Stripe-Like (YS/YSL) transporters (Hindt and Guerinot, 2012; Kobayashi *et al.*, 2019). Since Fe solubility increases with decreasing pH, and NH_4^+ uptake is known to provoke proton release to the apoplast and rhizosphere, ammonium nutrition has been shown to sometimes increase the absorption of nutrients such as P, Fe, or manganese (Mn) (Thomson *et al.*, 1993).

In the present work, we further studied plant adaptation to ammonium nutrition in *Brachypodium distachyon*, a widely accepted model for grasses and cereals (Kellogg, 2015). We mostly focused our effort at the root level, since it is the primary site of contact with NH_4^+ and may act as a physiological NH_4^+ barrier preventing its translocation to aerial parts (González-Moro *et al.*, 2021). To tackle this objective, we performed a proteomic analysis that, among others, revealed alterations of methionine (Met) metabolism and Fe homeostasis under ammonium nutrition. In general, we provide clear evidence of the close interaction between ammonium stress and Fe homeostasis in *B. distachyon*.

Materials and methods

Plant growth and experimental design

Brachypodium distachyon Bd21 plants were grown in hydroponic conditions as described by De la Peña *et al.* (2019). Briefly, 11-day-old seedlings were transferred to aerated hydroponic conditions and grown for 19 d with 1.25 mM $(NH_4)_2SO_4$ or 1.25 mM $Ca(NO_3)_2$ as N source. Nitrate-fed plants were supplemented with 1.25 mM $CaSO_4$ to balance the SO_4^{2-} supplied with the NH_4^+. For Fe deficiency treatment, plants were grown in hydroponic conditions for 7 d with optimal Fe supply [100 μM NaFe(III)-EDTA] and then subjected to Fe deprivation (–Fe) for 12 d. To maintain the pH stability and the concentration of mineral elements of the hydroponic medium, the nutrient solution was renewed on days 7, 11, 14, and 17. Plants were harvested between 10.00 h and 12.00 h (2 h after the onset of the photoperiod). Shoots and roots were separated and individually weighed. Plants grown in the same tank were pooled, immediately frozen in liquid nitrogen, homogenized in a Tissue Lyser (Retsch MM 400), and stored at –80 °C until use.

Proteomic analysis

A 10 mg aliquot of freeze-dried root powder was resuspended in 0.4 ml of 8 M urea, homogenized using a vortexer, and disrupted by sonication. After centrifugation at 13 000 *g*, the supernatant was collected. Protein integrity was checked by SDS precipitation with 2D CleanUp (GE Healthcare) according to the manufacturer's instructions, re-suspended in RapiGest 0.2% (Waters), and the protein concentration was determined (BCA assay; Thermo Fisher Scientific). A 75 μg aliquot of protein was heated (85 °C, 15 min), reduced with DTT (5 mM), alkylated with iodoacetamide (15 mM), and digested with trypsin (1.5 mg) overnight at

37 °C (Roche Diagnostics). RapiGest was inactivated twice by the addition of HCl at a final concentration of 0.5% and incubation at 37 °C for 40 min. Samples were centrifuged at 16 000 *g* for 10 min, the supernatant was collected, and 25 µg of protein was desalted using C-18 Micro SpinColums (Harvard Apparatus). Finally, samples were dried down in a SpeedVac centrifuge (ThermoFisher Scientific).

Mass spectrometry (MS) analyses were performed on an EASY-nLC 1200 liquid chromatography (LC) system interfaced with a Q Exactive HF-X mass spectrometer (ThermoFisher Scientific) via a nanospray flex ion source. Dried peptides were dissolved in 0.1% formic acid and loaded onto an Acclaim PepMap100 pre-column (75 µm×2 cm, ThermoFisher Scientific) connected to an Acclaim PepMap RSLC C18 (75 µm×25 cm, ThermoFisher Scientific) analytical column. Peptides were eluted in a linear gradient from 2% to 30% acetonitrile in 0.1% formic acid at a flow rate of 300 nl min^{-1} during 150 min. The mass spectrometer was operated in positive ion mode. Full MS scans were acquired from *m/z* 375 to 1800 with a resolution of 60 000 at *m/z* 200. The 15 most intense ions were fragmented by higher energy C-trap dissociation with a normalized collision energy of 28, and MS/MS spectra were recorded with a resolution of 15 000 at *m/z* 200. The maximum ion injection time was 60 ms for survey and MS/MS, whereas automatic gain control (AGC) target values were 3 × 106 and 5 × 105, respectively. In order to avoid repeat sequencing of peptides, dynamic exclusion was applied for 20 s. Singly charged ions or ions with an unassigned charge state were also excluded from MS/MS. Data were acquired using Xcalibur software (ThermoFisher Scientific).

Acquired raw data files were processed with the MaxQuant (Cox and Mann, 2008) software (version 1.6.0.16) using the internal search engine Andromeda (Cox *et al.*, 2011) and searched against the UniProt database restricted to *B. distachyon* entries (release 2017_08). Carbamidomethylation was set as a fixed modification, whereas Met oxidation and protein N-terminal acetylation were defined as variable modifications. Mass tolerance was set to 8 ppm and 20 ppm at the MS and MS/MS level, respectively. Enzyme specificity was set to trypsin, allowing for a maximum of three missed cleavages. Match between runs option was enabled with a 1.5 min match time window and a 20 min alignment window to match identification across samples. The false discovery rate (FDR) for peptides and proteins was set to 1%. Normalized spectral protein label-free quantification (LFQ) intensities were calculated using the MaxLFQ algorithm. MaxQuant output data were filtered with the Perseus module (version 1.6.0.7) (Tyanova *et al.*, 2016). Proteins identified by site (identification based only on a modified peptide), reserve proteins (identified by a decoy database), and potential contaminants were filtered out. Proteins with three LFQ values in at least one group were used for quantification, and missing LFQ intensity values were replaced with values from a normal distribution (width 0.3 and down shift 1.8), meant to simulate expression below the detection limit (Tyanova *et al.*, 2016).

Determination of metabolites

To quantify Met, *S*-methylmethionine (SMM), *S*-adenosylmethionine (SAM), *S*-adenosylhomocysteine (SAH), decarboxylated SAM (dc-SAM), and methylthioadenosine (MTA), 10 mg of tissue powder was homogenized in 500 µl of methanol:10 mM acetic acid (50:50, v/v) in a tissue homogenizer (FastPrep). Then 400 µl of the homogenate were mixed with 400 µl of chloroform and shaken for 60 min at 1400 rpm at 40 °C. Mixtures were then centrifuged for 30 min at 13 000 rpm and supernatants were evaporated in a SpeedVac. Pellets were resuspended in 150 µl of water:acetonitrile (40:60, v/v). Metabolites were quantified by LC:MS using a UPLC system (Acquity, Waters) coupled to time-of-flight (ToF) MS (SYNAPT G2 HDMS, Waters) in positive electrospray ionization (ESI) in full scan mode.

Nicotianamine (NA) and PSs [MA and analogous chelators: 2′-deoxymugineic acid (DMA), deoxydistichonic acid A (DDA), distichonic acid A (DA), avenic acid (AA), and 3-hydroxymugineic acid (HMA)] were quantified as described in Díaz-Benito *et al.* (2018). Briefly, 100 mg of tissue powder was extracted with 200 µl of ultrapure water containing nicotyl-lysine as internal standard. The homogenate was vortexed for 30 s, sonicated for 5 min, and centrifuged at 15 000 *g* for 10 min at 4 °C. The supernatant was recovered, filtered (3 kDa cellulose Amicon_ Ultra filter units, Merck KGaA), vacuum-dried, and the dry residues dissolved in 20 µl of ultrapure water. Aliquots of 5 µl of extracts were mixed with 25 µl of 20 mM EDTA and 30 µl of 10 mM ammonium acetate:acetonitrile (1:9, pH 7.3), and the mixture was filtered through a 0.45 µm polyvinylidene fluoride (PVDF) filter. Quantification was performed by LC:MS using an Alliance 2795 HPLC system (Waters) coupled to a ToF mass spectrometer (MicrOTOF, Bruker Daltonics) equipped with an ESI source. Pure NA and DMA were used as standards.

NH_4^+ was extracted from 20 mg of frozen shoot and root powder in 650 µl of ultrapure water, homogenized at 27 Hz for 1 min, heated at 80 °C for 5 min, centrifuged at 4000 *g* for 20 min, and the supernatant recovered. The quantification was performed following the phenol hypochlorite method in a 96-well microplate reader (Sarasketa *et al.*, 2016).

Chlorophyll was quantified spectrophotometrically from shoot tissue extracted in 80% aqueous acetone as described in De la Peña *et al.* (2019).

Fe and zinc (Zn) were extracted from 10 mg of freeze-dried shoot and root with HNO_3 by microwave-assisted digestion (Mars6, Vertex) and quantified by inductively connected plasma MS (ICP-MS; Thermo Fisher Scientific).

Gene expression analysis

RNA extraction was carried out from 25 mg of frozen shoot or root powder with the Nucleospin RNA plant kit (Macherey-Nagel) that includes DNase treatment. A 1 µg aliquot of RNA was retrotranscribed into cDNA (PrimeScript™ RT; Takara Bio) and gene expression was determined from 2 µl of cDNA diluted 1:10 in a 15 µl reaction volume using SYBR Premix ExTaq™ (Takara Bio) in a Step One Plus Real Time PCR System (Applied Biosystems). *ACT3* and *UBC18* were used as housekeeping genes to normalize gene expression. Absence of genomic DNA contamination was checked in all RNA samples. Primers used are described in Supplementary Table S1.

Statistical analysis

Data were analysed with SPSS 17.0 (Chicago, IL, USA) or R software v. 3.4.4. Normality and homogeneity of variance were analysed by Kolmogorov–Smirnov and Levene's tests. Student's *t*-tests or one-way ANOVA followed by a Duncan post-hoc test were used to compare sample groups. Non-normally distributed data were analysed with the Mann–Whitney U-test for non-parametric data.

Results

Ammonium nutrition impacts root primary metabolism, redox balance, and cell wall biogenesis

Ammonium nutrition often reduces plant growth, and that is also the case for *B. distachyon* (Supplementary Table S2; De La Peña *et al.*, 2019; Glazowska *et al.*, 2019). To further understand root adaptation to ammonium nutrition, we carried out a label-free quantitative proteomic study and analysed the relative abundance of proteins in *B. distachyon* roots grown under ammonium or nitrate nutrition. A total of 4506 distinct proteins were identified with an FDR <1% (Supplementary

Table S3), and 4109 were quantified. Of these, 475 showed differential abundance, with a significant level of $P < 0.05$ and 1.5-fold change (FC) cut-off, where 243 proteins presented higher abundance in roots of ammonium-grown plants and 232 higher abundance in roots of nitrate-grown plants (Supplementary Table S3; Supplementary Fig. S1). Biological process Gene Ontology enrichment analysis (PANTHER 14.1; www.pantherdb.org) revealed 139 significantly enriched functional classes (Fisher's exact test $P \leq 0.0$; Benjamini–Hochberg FDR ≤0.05), 68 with up- and 71 with down-regulated proteins (Supplementary Table S4).

In Fig. 1A, B, the most specific over-represented functional classes are shown. As reported in many species including *B. distachyon* (De la Peña *et al.*, 2019; González-Moro *et al.*, 2021), the N source had a great impact on root primary metabolism. In agreement with this, enriched classes were related to C and N metabolism (e.g. glycolytic process, carbohydrate metabolic process, or carboxylic acid catabolic process). Among others, proteome data corroborated the down-regulation of GS2 ('glutamine synthetase chloroplastic' I1J2T4) already observed in ammonium-fed *B. distachyon* at the gene expression level (De la Peña *et al.*, 2019) and in other species, such as Arabidopsis (Sarasketa *et al.*, 2016). The up-regulation of asparagine synthetase (I1IV86) is also in agreement with the huge root Asn accumulation reported in De la Peña *et al.* (2019). Moreover, GDH2 (I1J084), a classical marker of plant response to ammonium nutrition (Loulakakis and Roubelakis-Angelakis, 1991; González-Moro *et al.*, 2021), was up-regulated in roots of ammonium-fed *B. distachyon* plants (Supplementary Table S3). Regarding C metabolism enzymes, among others, pyruvate kinase (I1HEH4), a cytosolic triose phosphate isomerase (I1HC04), hexokinase (A0A0Q3IMN1), and citrate synthase (I1HYA2) were up-regulated under ammonium nutrition (Supplementary Table S3).

Besides C and N metabolism, enriched categories highlighted cell redox balance (e.g. 'response to oxidative stress', 'cellular oxidant detoxification') and cell wall biogenesis and metabolism ('cinnamic acid biosynthetic process', 'L-Phe catabolic process'). Cell wall remodelling is key for cell expansion; loosening of the wall allows the cell to expand, whereas cross-linking between their polymers inhibits cell expansion. Several reports have shown a relationship between ammonium nutrition and cell wall biogenesis and organization (Podgórska *et al.*, 2017; Glazowska *et al.*, 2019; Royo *et al.*, 2019). In our work, we found decreased abundance of three xyloglucan endotransglucosylase/hydrolases (XTHs) in ammonium-fed roots (I1I257, I1I258, and I1IGTU3) and proteins associated with phenylpropanoid biosynthesis including lignin; among others, three phenylalanine ammonia lyase enzymes, a probable 4-coumarate-CoA ligase 3 (I1IHXV5), and a caffeoyl-CoA *O*-methyltransferase 1 (I1H0Q2) (Supplementary Table S2). Indeed, Royo *et al.* (2019) showed differential abundance of cell wall-associated proteins and higher lignin deposition in *Medicago truncatula* plants grown in ammonium nutrition. In addition, Podgórska *et al.* (2017) reported higher cell wall stiffness under ammonium nutrition, overall suggesting that NH_4^+-mediated growth inhibition could be related to a more rigid cell wall structure.

Ammonium nutrition enhances the Met cycle and the synthesis of phytosiderophores, leading to Fe accumulation

Among the functional classes over-represented when analysing the proteins with higher abundance in ammonium-fed plants, categories related to the Met salvage cycle and NA biosynthesis ('L-methionine salvage from methylthioadenosine', '*S*-adenosylmethionine biosynthetic process', 'nicotianamine biosynthetic process') were those with the highest fold enrichment (Fig. 1B; Supplementary Table S4). Indeed, enzymes of almost every step of the Met salvage cycle were up-regulated with ammonium nutrition (Figs 1C, 2).

The Met salvage cycle and NA biosynthesis are related to the synthesis of PSs, and thus to the uptake of metals, notably Fe and Zn (Kobayashi *et al.*, 2005). In agreement with this, 20 proteins related to Fe homeostasis were found to be regulated by the N source (Fig. 1C). We confirmed this result by analysing the expression of nine protein-encoding genes (Supplementary Fig. S2), selected among the 20 Fe-related proteins (Fig. 1C). Thus, we focused on better understanding the impact of ammonium nutrition on Met-associated pathways and complemented the proteome data with an in-depth quantification of Met/SAM derivatives, NA, and PSs by LC:MS.

In agreement with the proteome profile, striking differences were found in the content of most metabolites analysed as a function of the N source provided. Ammonium nutrition provoked a decrease in root Met content and in the SAM derivatives SAH, dcSAM, and MTA, while SAM content did not vary. In contrast, SMM content increased in ammonium-fed roots (Fig. 2). The effect of the nutrition type on these compounds in shoots was similar to that in roots (Supplementary Fig. S3). Regarding PS content, five out six of the MAs were higher in ammonium nutrition (Fig. 2). Among them, the content of MA, which represented ~90% of the total content of MAs, was 7.6-fold higher under ammonium nutrition. Moreover, the accumulation of NA was 13.5-fold higher under ammonium with respect to nitrate nutrition. Both proteome data and PS analysis clearly suggested a potential increase of Fe uptake in ammonium-fed plants. Accordingly, the content of Fe was higher in the root of plants grown with NH_4^+ with respect to those grown with NO_3^- supply (Fig. 3).

The nitrogen source influences B. distachyon *response to Fe deficiency*

Due to the finding of the higher root PS and Fe content under ammonium nutrition, we hypothesized that *B. distachyon* response to Fe deficiency could be altered as a function of the

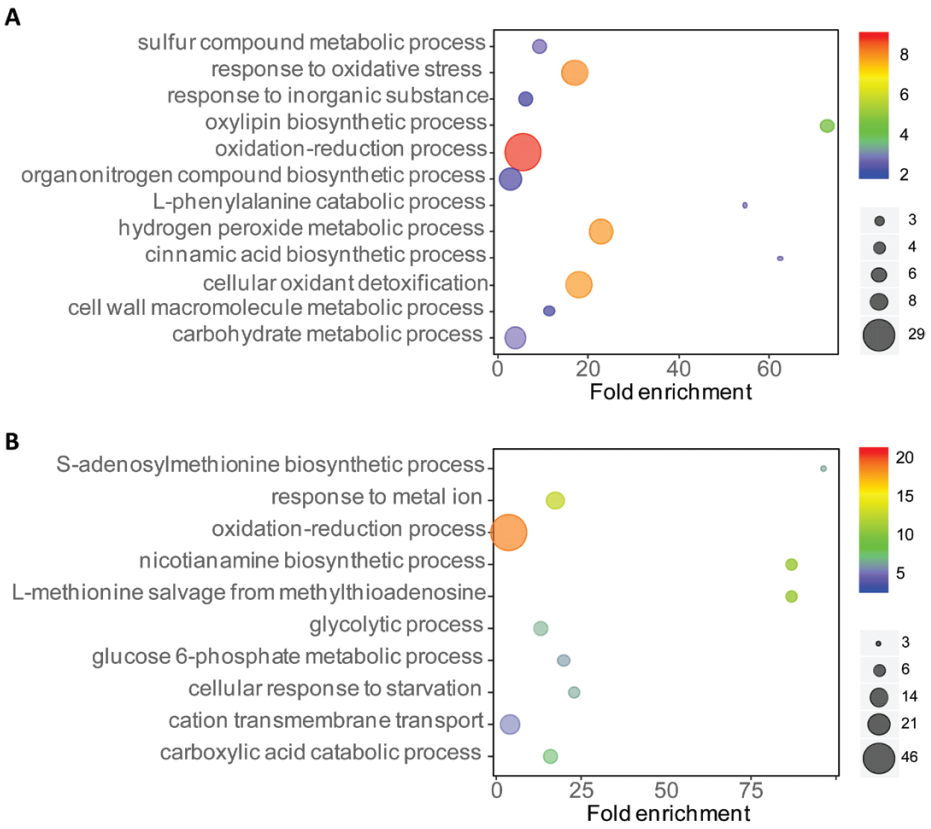

C

Uniprot code	Gene ID	Protein description	log_2FC (-4.7 0 3.6)
I1HF18	LOC100843457	S-Adenosylmethionine synthase 1	1.22
I1HF17	LOC100844978	S-Adenosylmethionine synthase 3-like	0.99
I1H1W0	LOC100839737	5'-Methylthioadenosine/S-adenosylhomocysteine nucleosidase 2-like	1.00
I1IMJ2	LOC100834960	Methylthioribose-1-phosphate isomerase	1.60
I1IES2	LOC100828599	Probable bifunctional methylthioribulose-1-phosphate dehydratase	1.87
I1J366	LOC100837535	Methylthioribose kinase 2	1.93
I1GTE3	LOC100837759	1,2-dihydroxy-3-keto-5-methylthiopentene dioxygenase 2	2.15
I1IAD2	LOC100829217	Nicotianamine synthase-like 5 protein	2.50
I1HZL5	LOC100822873	Nicotianamine synthase 2-like	2.52
I1H680	LOC100832895	Probable nicotianamine synthase 2	1.18
I1HZX5	LOC100831451	Nicotianamine aminotransferase A-like	3.60
I1GYH1	LOC100822209	Nicotianamine aminotransferase A-like	0.74
I1IL44	LOC100841166	Nicotianamine aminotransferase A-like	0.68
I1IUR4	LOC100823408	2'-Deoxymugineic-acid 2'-dioxygenase-like	2.67
I1J071	LOC100826305	Probable metal-nicotianamine transporter YSL9-like	3.52
I1IP67	LOC100837011	Ferrochelatase-2, chloroplastic	0.95
I1H8C0	LOC100845842	Metal transporter Nramp2	1.40
I1IV67	LOC100837024	Ferritin-1, chloroplastic	-4.67
I1GUN7	LOC100837457	CDGSH iron-sulfur domain-containing protein NEET	-2.41
I1HBL2	LOC100825497	Uncharacterized protein (SUF_FeS_clus_asmbl_SufBD)	-1.07

Fig. 1. Gene Ontology enrichment analysis of proteins with lower (A) and higher abundance (B) in ammonium-fed with respect to nitrate-fed *B. distachyon* plants. Only the most specific significant categories are represented. The colour scale represents the $-\log_{10}$(*P*-value), and dot size indicates the number of proteins. (C) Proteins related to iron homeostasis displaying differential abundance as a function of the N source provided.

N source provided. To test this hypothesis, we subjected plants adapted to ammonium or nitrate nutrition to Fe deficiency (–Fe). As expected, we found that –Fe condition provoked a substantial decrease in plant growth and chlorophyll content independently of the N source provided (Fig. 4). However, root growth inhibition provoked by ammonium nutrition was more evident in Fe deficiency, with root biomass being reduced by 26% in control conditions and by 40% under Fe

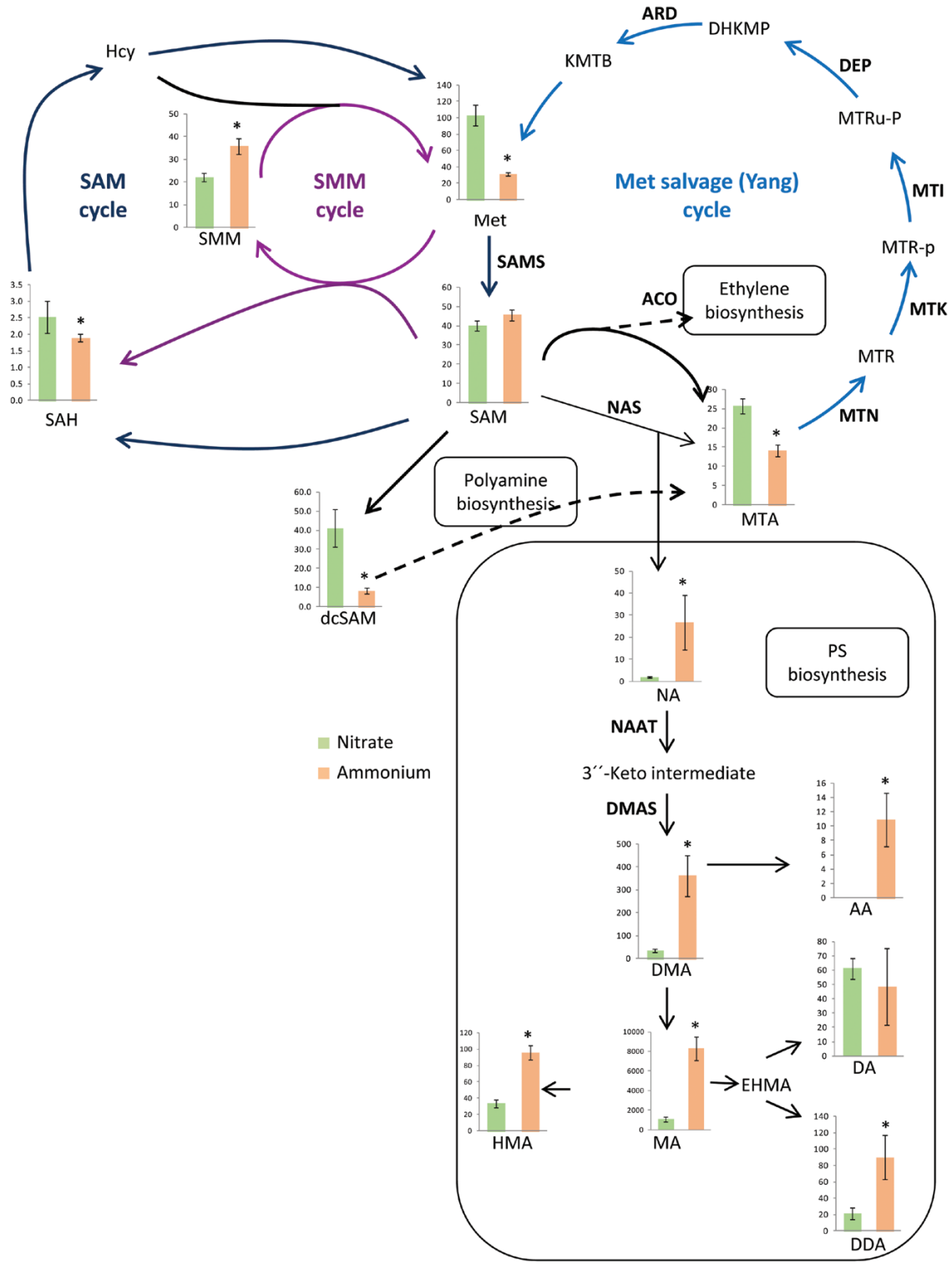

Fig. 2. Content of Met/SAM derivatives, NA, and PSs in roots of *B. distachyon* grown under ammonium or nitrate nutrition. Columns represent the mean values ±SE (n=4) expressed in nmol g FW^{-1}, except for dcSAM which is given in relative units. An asterisk indicates significance differences between the N source analysed (P<0.05). Enzymes shown in the diagram are those that displayed significantly higher abundance under ammonium nutrition in the proteomic analysis. AA, avenic acid; ACO, 1-aminocyclopropane-1-carboxylate oxidase; ARD, acireductone dioxygenase or 2-keto-methylthiobutyric acid-forming enzyme; DA, distichonic acid A; dcSAM, decarboxylated SAM; DDA, deoxydistichonic acid A; DEP, methylthioribulose-1-phosphate dehydratase-enolase-phosphatase; DHKMP, 1,2-dihydro-3-keto-5- methylthiopentene; DMA, 2′-deoxymugineic acid; EHMA, 3-epi-hydroxy-mugineic acid; Hcy, homocysteine; HMA, 3-hydroxymugineic acid; KMTB, 2-oxo-4-methylthiobutyrate; MA, mugineic acid; Met, methionine;

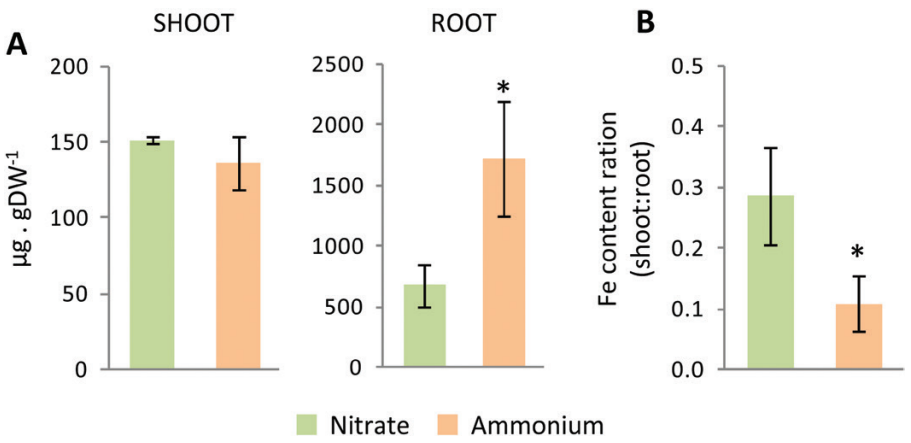

Fig. 3. Fe content in shoots and roots (A) and Fe content ratio (B) of *B. distachyon* grown under ammonium or nitrate nutrition. Columns represent the mean values ±SE (n=4). An asterisk indicates a significance difference between the N source analysed (P<0.05).

deficiency in ammonium-fed compared to nitrate-fed plants (Fig. 4). Importantly, this lower growth under Fe deficiency was not due to impaired Fe uptake, since Fe content was higher under ammonium nutrition compared with nitrate nutrition (Fig. 5A). In agreement with PS synthesis induction, Zn content was greatly increased with ammonium nutrition under Fe deficiency (Fig. 5B). Overall, the results suggest that although Fe uptake is increased in ammonium nutrition, Fe availability is compromised. Indeed, the fact that the content of the cellular Fe storage protein ferritin was ~25 times lower in roots under ammonium nutrition ($\log_2$ FC −4.67) supports this hypothesis (Fig. 1C). In addition, the exclusive accumulation of Fe at the root level (Figs 3–5) suggests that Fe root to shoot transport may be compromised under ammonium nutrition.

We analysed by quantitative PCR (qPCR) the expression of marker genes associated with Fe deficiency and observed that most genes were already induced in Fe-supplied (control) ammonium-fed plants (Fig. 6; Supplementary Fig. S4). In roots, the higher *FRLD1*, *IDEF2*, and *YSL2* expression compared with nitrate-fed plants was maintained under Fe deficiency (Fig. 6). Root *NAAT* and *DMAS* expression did not respond to Fe deprivation under ammonium nutrition since their expression was already maximal under control conditions. Also, in agreement with ferritin content (Fig. 1C), *FER1* gene expression was lower in ammonium-fed plants in both roots and shoots (Fig. 6; Supplementary Fig. S4).

Finally, we determined NH_4^+ accumulation, a classic marker of ammonium stress. Interestingly, Fe deficiency greatly enhanced NH_4^+ accumulation, notably at the root level (Fig. 7A), which in turn was correlated with higher amino acid abundance (Fig. 7B). Overall, as suggested by the proteomic study, physiological data and micronutrient analysis confirm the close interaction between Fe homeostasis and ammonium nutrition in *B. distachyon*.

Discussion

Ammonium nutrition provoked a clear induction of Fe-deficiency responses in *B. distachyon*, as evidenced by the stimulation of the Met salvage cycle and PS synthesis (Figs 1, 2), together with the higher expression of Fe deficiency-responsive genes (Fig. 6; Supplementary Fig. S4). Graminaceous species take up Fe following a chelation-based strategy (commonly known as Strategy II) and, as a consequence, Fe deficiency stimulates the synthesis of PSs (NA and MAs). NA is synthesized by NA synthase (NAS) from the combination of three units of SAM. In addition, SAM is the precursor of many other biomolecules such as polyamines and ethylene. In these reactions, such as NA synthesis, MTA is released and can be recycled again to Met or SAM thanks to the Met salvage cycle, also known as the Yang cycle (Kobayashi *et al.*, 2005; Sauter *et al.*, 2013). Indeed, the Met salvage cycle is highly active in the root and it is also induced under Fe deficiency to enable this organ to meet the increased demand for SAM required for the synthesis of MAs (Ma *et al.*, 1995; Kobayashi *et al.*, 2005).

To sustain PS synthesis, Strategy II plants need proper SAM availability, which demands sulfate (SO_4^{2-}) uptake and assimilation. These two processes have been suggested to increase under ammonium nutrition (Van Beusichem *et al.*, 1988; Gerendás *et al.*, 1997; Coleto *et al.*, 2017). Following this same line of evidence, ammonium-fed *B. distachyon* roots displayed higher abundance of ATP sulfurylase 1 (I1GNF6) and other sulfur-related proteins under ammonium nutrition (Supplementary

MTA, 5-methylthioadenosine; MTI, 5-methylthioribose-1-phosphate isomerase; MTK, 5-methylthioribose kinase; MTN, MTA nucleosidase; MTR, 5-methylthioribose; MTR-P, 5-methylthioribose-1-phosphate; MTRu-P, 5-methylthioribulose-phosphate; NA, nicotianamine; NAAT, NA-aminotransferase; NAS, nicotianamine synthase; PS, phytosiderophore; SAH, *S*-adenosylhomocysteine; SAM, *S*-adenosyl-Met; SAMS, *S*-adenosyl-Met synthetase; SMM, *S*-methylmethionine.

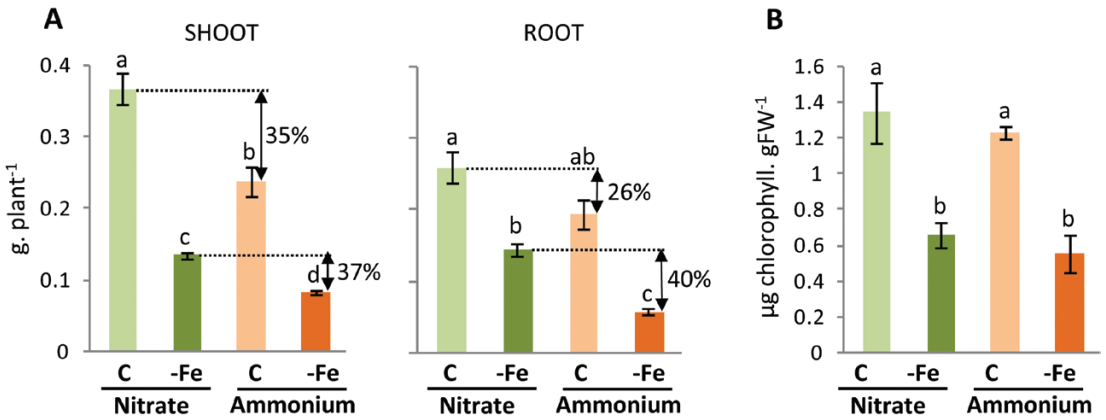

Fig. 4. Biomass and chlorophyll content of *B. distachyon*. Biomass (A) and chlorophyll content (B) of *B. distachyon* grown under ammonium or nitrate nutrition under control (C) or Fe deficiency (–Fe) conditions. Columns represent the mean values ±SE (n=30 for biomass, n=6 for chlorophyll). Different letters indicate significant differences according to one-way ANOVA followed by Duncan's test (P<0.05).

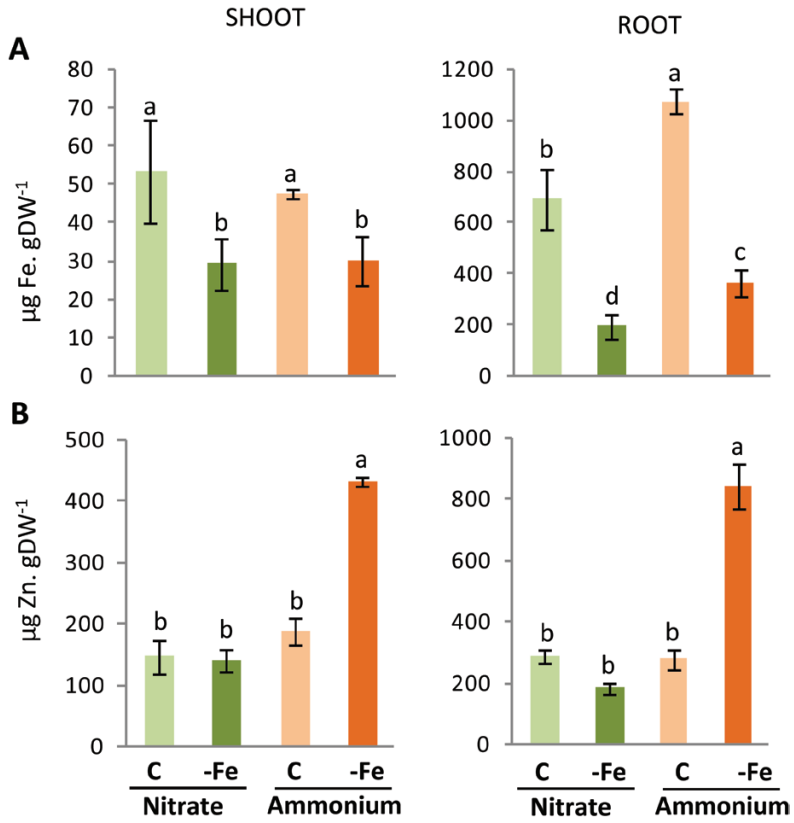

Fig. 5. Iron and zinc content in *B. distachyon*. Iron (A) and zinc (B) content in *B. distachyon* grown under ammonium or nitrate nutrition under control (C) or Fe deficiency (–Fe) conditions. Columns represent mean values ±SE (n=3). Different letters indicate significant differences according to one-way ANOVA followed by Duncan's test (P<0.05).

Table S3). Indeed, while most SAM intermediates were reduced in ammonium-fed plants, SAM content remained equal to that of nitrate-fed plants (Fig. 2; Supplementary Fig. S3). Interestingly, despite the Met level being reduced, the SMM content increased under ammonium nutrition (Fig. 2; Supplementary Fig. S3). SMM is considered to be the mobile and storage form of Met and may also be involved in the tolerance of plants to abiotic stresses (Ogawa and Mitsuya, 2012). The reason the SMM level increases while that of other Met/SAM derivatives decreases is unknown and is a question to be tackled in future studies.

As expected in view of the striking enhancement of PS synthesis, root Fe content increased in the root of ammonium-fed plants (Fig. 3). Stimulation of Fe uptake by NH_4^+ supply has

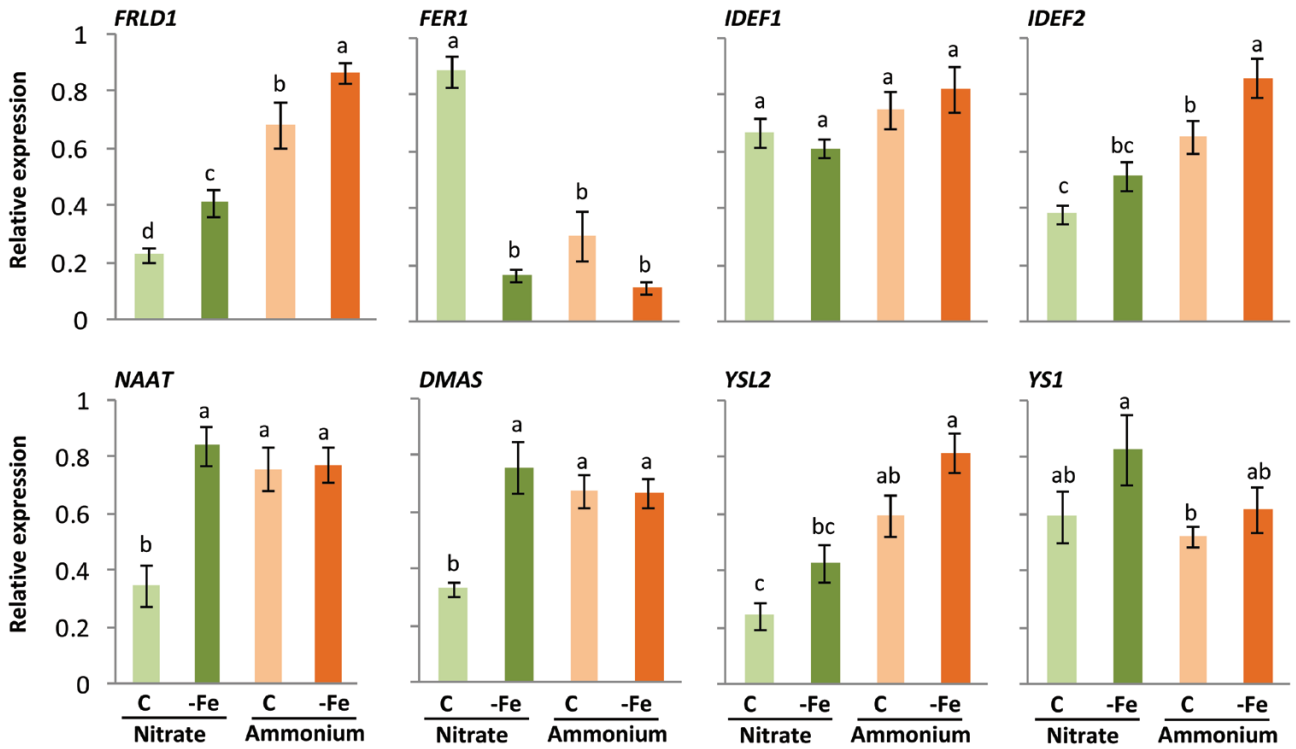

Fig. 6. Expression of Fe-related genes in roots of *B. distachyon* grown under ammonium or nitrate nutrition under control (C) or Fe deficiency (–Fe) conditions. Columns represent the mean values ±SE (n=6). Different letters indicate significant differences according to one-way ANOVA followed by Duncan's test (P<0.05).

sometimes been associated with an increase of Fe^{3+} solubility because of ammonium-induced apoplast/rhizosphere acidification (Mengel and Geurtzen, 1988; Alloush *et al.*, 1990; Kosegarten and Englisch, 1994; Kosegarten *et al.*, 1998). In our work, the nutrient solution was buffered and renewed every 3–4 d, the medium pH remaining quite stable (6.9–7.4) during the whole experiment. Similarly, other authors also indicate that pH acidification of the rhizosphere is unlikely to be the sole reason for the Fe uptake stimulation observed under ammonium nutrition (Zhu *et al.*, 2018, 2019). Therefore, it appears clear that the higher Fe levels found *in B. distachyon* are associated with enhanced PS synthesis rather than with a pH-related increase of Fe solubility.

Despite higher root Fe content, ammonium-fed *B. distachyon* plants displayed increased root sensitivity to Fe deficiency (Fig. 4). Thus, it appears that the accumulated Fe in *B. distachyon* roots would not be available for use by the cell or that the plant's capacity to use the absorbed Fe is compromised. In consequence, Fe deficiency responses including the Fe uptake machinery would be induced. Among others causes, reduced Fe availability could be due to an incorrect loading of the Fe from the xylem/apoplast into the cells or to perturbations in subcellular partitioning of Fe (Haydon *et al.*, 2012). In this same line of evidence, lower ferritin content was also found in a proteome analysis performed in ammonium-fed *Medicago truncatula* plants (Royo *et al.*, 2019). In addition, ammonium nutrition has also been observed to stimulate Fe deficiency responses in Arabidopsis (Zhu *et al.*, 2019; Coleto *et al.*, 2021). Indeed, recently we reported that altered Fe homeostasis could be associated with the Arabidopsis response to ammonium nutrition through a signalling pathway involving MYB28 and MYB29 transcription factors (Bejarano *et al.*, 2021; Coleto *et al.*, 2021). However, in contrast to the observed *B. distachyon* root growth decrease in ammonium-fed plants under Fe deficiency, several works reported a beneficial effect of NH_4^+ supply in response to Fe deprivation (Alloush *et al.*, 1990; Kosegarten and Englisch, 1994; Kosegarten *et al.*, 1998; Zou *et al.*, 2001; Zhu *et al.*, 2018, 2019). In these studies, ammonium plants were not grown under ammonium stress conditions, and thus we can hypothesize that the differences found may be associated with the degree of ammonium stress. Alternatively, a species-dependent response cannot be ruled ou.

Fe deficiency also provoked a striking increase of root NH_4^+ content (Fig. 7). Similarly, in Arabidopsis, Fe deficiency also induced NH_4^+ uptake, which was correlated with the induction of the expression of *AMT1;1* and *AMT1;3* NH_4^+ transporter genes (Zhu *et al.*, 2019). Since excessive NH_4^+ accumulation in tissues is generally known to be detrimental for plant performance (Britto and Kronzucker, 2002; González-Moro *et al.*, 2021), the negative effect of NH_4^+ accumulation on root growth under Fe deficiency cannot be ignored. In addition, the high levels of Zn observed in ammonium-fed plants under Fe deficiency, associated with the stimulation of PSs combined

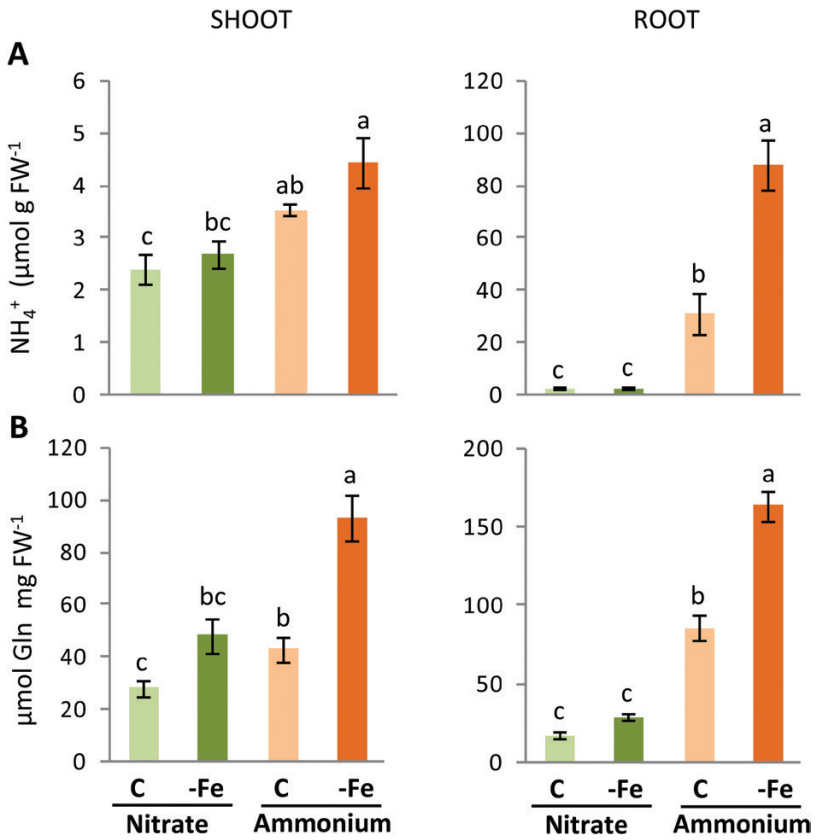

Fig. 7. Ammonium (A) and total free amino acid (B) content in *B. distachyon* grown under ammonium or nitrate nutrition under control (C) or Fe deficiency (–Fe) conditions. Columns represent the mean values ±SE (n=6). Different letters indicate significant differences according to one-way ANOVA followed by Duncan's test (P<0.05).

with the absence of Fe to compete for these PSs, could be also detrimental for plant growth. Indeed, Zn phytotoxicity symptoms typically appear when Zn accumulates in the shoot in the 300–1000 ppm range (Chaney, 1993).

Altogether, in this work, we show that the adaptation of *B. distachyon* roots to ammonium nutrition involves changes in C and N metabolism, cell wall metabolism, redox homeostasis and interaction with other ions. In particular, PS synthesis was enhanced under ammonium nutrition, leading to increased Fe uptake. In addition, the interaction between ammonium nutrition and Fe metabolism was evidenced by the increased sensitivity of ammonium-fed plants to Fe deficiency. Overall, the results suggest that ammonium nutrition triggers impaired Fe utilization and transport. Future research is needed to further elucidate the mechanisms underlying the interaction between Fe and NH_4^+, notably regarding the mechanism leading to Fe unavailability for use by the cell, in order to better understand and improve ammonium use efficiency and tolerance in plants.

Supplementary data

The following supplementary data are available at *JXB* online.

Table S1. Primers used for qPCR gene expression analysis.

Table S2. Biomass and chlorophyll content of *Brachypodium distachyon* plants grown under ammonium or nitrate nutrition.

Table S3. List of proteins identified, quantified, and differentially expressed in roots of *B. distachyon* grown under nitrate or ammonium nutrition.

Table S4. Full list of enriched GO functional classes.

Fig. S1. Volcano plot of the quantified proteins.

Fig. S2. Expression of selected genes encoding proteins related to iron homeostasis displaying differential abundance (see Fig. 1C) in the roots of *B. distachyon* grown under ammonium or nitrate nutrition.

Fig. S3. Met/SAM derivatives in shoots of *B. distachyon* grown under ammonium or nitrate nutrition.

Fig. S4. Expression of Fe-related genes in the shoot of *B. distachyon* grown under ammonium or nitrate nutrition under control (C) or Fe deficiency (–Fe) conditions

Acknowledgements

We thank Diana Cabrera from C.I.C. bioGUNE for technical assistance in Met cycle analysis, and we are grateful for the technical and human support provided by SGIker (UPV/EHU).

Author contributions

MBGM and DM: conceptualization and supervision; MP, AJMP, LU, IC, and DM: performing the experiments and data analysis; SML and JMFP: quantifying Met derivatives; JCG and AAF: quantifying PSs; MP and DM: writing. All authors edited and approved the final manuscript.

Funding

This research was funded/supported by the Basque Government (IT932-16) and the Spanish Ministry of Economy and Competitiveness (BIO2017-84035-R and PID2020-113385RB-I00 co-funded by FEDER). MP held a doctoral scholarship (Conv. 672) associated with COLCIENCIAS (Department of Science, Technology and Innovation of Colombia) and the Department of Magdalena. LU holds a PhD grant from the Basque Government and AJMP from the Spanish Ministry of Economy and Competitiveness.

Data availability

All data supporting the findings of this study are available within the paper and within its supplementary data published online.

References

Alloush GA, Bot JL, Sanders FE, Kirkby EA. 1990. Mineral nutrition of chickpea plants supplied with NO_3^- or NH_4^+ N. I. Ionic balance in relation to iron stress. Journal of Plant Nutrition **13**, 1575–1590.

Balkos KD, Britto DT, Kronzucker HJ. 2010. Optimization of ammonium acquisition and metabolism by potassium in rice (*Oryza sativa* L. cv. IR-72). Plant, Cell & Environment **33**, 23–34.

Beeckman F, Motte H, Beeckman T. 2018. Nitrification in agricultural soils: impact, actors and mitigation. Current Opinion in Biotechnology **50**, 166–173.

Bejarano I, Marino D, Coleto I. 2021. Arabidopsis MYB28 and MYB29 transcription factors are involved in ammonium-mediated alterations of root-system architecture. Plant Signaling & Behavior **16**, 1879532.

Bouain N, Krouk G, Lacombe B, Rouached H. 2019. Getting to the root of plant mineral nutrition: combinatorial nutrient stresses reveal emergent properties. Trends in Plant Science **24**, 542–552.

Briat JF, Dubos C, Gaymard F. 2015. Iron nutrition, biomass production, and plant product quality. Trends in Plant Science **20**, 33–40.

Britto DT, Kronzucker HJ. 2002. NH_4^+ toxicity in higher plants: a critical review. Journal of Plant Physiology **584**, 567–584.

Chaney RL. 1993. Zinc phytotoxicity. In: Robson AD, ed. Zinc in soils and plants. Dordrecht: Springer Science+Business Media, 135–144.

Coleto I, Bejarano I, Marín-Peña AJ, Medina J, Rioja C, Burow M, Marino D. 2021. *Arabidopsis thaliana* transcription factors *MYB28* and *MYB29* shape ammonium stress responses by regulating Fe homeostasis. New Phytologist **229**, 1021–1035.

Coleto I, de la Peña M, Rodríguez-Escalante J, Bejarano I, Glauser G, Aparicio-Tejo PM, González-Moro MB, Marino D. 2017. Leaves play a central role in the adaptation of nitrogen and sulfur metabolism to ammonium nutrition in oilseed rape (*Brassica napus*). BMC Plant Biology **17**, 1–13.

Coskun D, Britto DT, Kronzucker HJ. 2014. The physiology of channel-mediated K^+ acquisition in roots of higher plants. Physiologia Plantarum **151**, 305–312.

Cox J, Mann M. 2008. MaxQuant enables high peptide identification rates, individualized p.p.b.-range mass accuracies and proteome-wide protein quantification. Nature Biotechnology **26**, 1367–1372.

Cox J, Neuhauser N, Michalski A, Scheltema RA, Olsen JV, Mann M. 2011. Andromeda: a peptide search engine integrated into the MaxQuant environment. Journal of Proteome Research **10**, 1794–1805.

Cui YN, Li XT, Yuan JZ, Wang FZ, Wang SM, Ma Q. 2019. Nitrate transporter NPF7.3/NRT1.5 plays an essential role in regulating phosphate deficiency responses in Arabidopsis. Biochemical and Biophysical Research Communications **508**, 314–319.

De la Peña M, González-Moro MB, Marino D. 2019. Providing carbon skeletons to sustain amide synthesis in roots underlines the suitability of *Brachypodium distachyon* for the study of ammonium stress in cereals. AoB Plants **11**, plz029.

Díaz-Benito P, Banakar R, Rodríguez-Menéndez S, Capell T, Pereiro R, Christou P, Abadía J, Fernández B, Álvarez-Fernández A. 2018. Iron and zinc in the embryo and endosperm of rice (*Oryza sativa* L.) seeds in contrasting 2′-deoxymugineic acid/nicotianamine scenarios. Frontiers in Plant Science **9**, 1190.

Gerendás J, Zhu Z, Bendixen R, Ratcliffe RG, Sattelmacher B. 1997. Physiological and biochemical processes related to ammonium toxicity in higher plants. Zeitschrift für Pflanzenernährung und Bodenkunde **160**, 239–251.

Glazowska S, Baldwin L, Mravec J, Bukh C, Fangel JU, Willats WG, Schjoerring JK. 2019. The source of inorganic nitrogen has distinct effects on cell wall composition in *Brachypodium distachyon*. Journal of Experimental Botany **70**, 6461–6473.

González-Moro MB, González-Moro I, de la Peña M, Estavillo JM, Aparicio-Tejo PM, Marino D, González-Murua C, Vega-Mas I. 2021. A multi-species analysis defines anaplerotic enzymes and amides as metabolic markers for ammonium nutrition. Frontiers in Plant Science **11**, 632285.

Haydon MJ, Kawachi M, Wirtz M, Hillmer S, Hell R, Krämer U. 2012. Vacuolar nicotianamine has critical and distinct roles under iron deficiency and for zinc sequestration in Arabidopsis. The Plant Cell **24**, 724–737.

Hindt MN, Guerinot ML. 2012. Getting a sense for signals: regulation of the plant iron deficiency response. Biochimica et Biophysica Acta **1823**, 1521–1530.

Huérfano X, Estavillo JM, Fuertes-Mendizábal T, Torralbo F, González-Murua C, Menéndez S. 2018. DMPSA and DMPP equally reduce N_2O emissions from a maize–ryegrass forage rotation under Atlantic climate conditions. Atmospheric Environment **187**, 255–265.

Kellogg EA. 2015. *Brachypodium distachyon* as a genetic model system. Annual Review of Genetics **49**, 1–20.

Kobayashi T, Nozoye T, Nishizawa NK. 2019. Iron transport and its regulation in plants. Free Radical Biology & Medicine **133**, 11–20.

Kobayashi T, Suzuki M, Inoue H, Itai RN, Takahashi M, Nakanishi H, Mori S, Nishizawa NK. 2005. Expression of iron-acquisition-related genes in iron-deficient rice is co-ordinately induced by partially conserved iron-deficiency-responsive elements. Journal of Experimental Botany **56**, 1305–1316.

Kosegarten H, Englisch G. 1994. Effect of various nitrogen forms on the pH in leaf apoplast and on iron chlorosis of *Glycine max* L. Zeitschrift für Pflanzenernährung und Bodenkunde **157**, 401–405.

Kosegarten H, Schwed U, Wilson G, Mengel K. 1998. Comparative investigation on the susceptibility of faba bean (*Vicia faba* L.) and sunflower (*Helianthus annuus* L.) to iron chlorosis. Journal of Plant Nutrition **21**, 1511–1528.

Loulakakis KA, Roubelakis-Angelakis KA. 1991. Plant NAD(H)-glutamate dehydrogenase consists of two subunit polypeptides and their participation in the seven isoenzymes occurs in an ordered ratio. Plant Physiology **97**, 104–111.

Ma JF, Shinada T, Matsuda C, Nomoto K. 1995. Biosynthesis of phytosiderophores, mugineic acids, associated with methionine cycling. Journal of Biological Chemistry **270**, 16549–16554.

Marschner H. 2012. Marschner's mineral nutrition of higher plants. New York: Academic Press.

Medici A, Marshall-Colon A, Ronzier E, Szponarski W, Wang R, Gojon A, Crawford NM, Ruffel S, Coruzzi GM, Krouk G. 2015. AtNIGT1/

HRS1 integrates nitrate and phosphate signals at the Arabidopsis root tip. Nature Communications **6**, 6274.

Mengel K, Geurtzen G. 1988. Relationship between iron chlorosis and alkalinity in *Zea mays*. Physiologia Plantarum **72**, 460–465.

Ogawa S, Mitsuya S. 2012. S-methylmethionine is involved in the salinity tolerance of *Arabidopsis thaliana* plants at germination and early growth stages. Physiologia Plantarum **144**, 13–19.

Podgórska A, Burian M, Gieczewska K, Ostaszewska-Bugajska M, Zebrowski J, Solecka D, Szal B. 2017. Altered cell wall plasticity can restrict plant growth under ammonium nutrition. Frontiers in Plant Science **8**, 1344.

Ricachenevsky FK, Sperotto RA. 2014. There and back again, or always there? The evolution of rice combined strategy for Fe uptake. Frontiers in Plant Science **5**, 189.

Roosta HR, Schjoerring JK. 2007. Effects of ammonium toxicity on nitrogen metabolism and elemental profile of cucumber plants. Journal of Plant Nutrition **30**, 1933–1951.

Royo B, Esteban R, Buezo J, Santamaría E, Fernández-Irigoyen J, Becker D, Moran JF. 2019. The proteome of *Medicago truncatula* in response to ammonium and urea nutrition reveals the role of membrane proteins and enzymes of root lignification. Environmental and Experimental Botany **162**, 168–180.

Sarasketa A, González-Moro MB, González-Murua C, Marino D. 2016. Nitrogen source and external medium pH interaction differentially affects root and shoot metabolism in Arabidopsis. Frontiers in Plant Science **7**, 29.

Sauter M, Moffatt B, Saechao MC, Hell R, Wirtz M. 2013. Methionine salvage and S-adenosylmethionine: essential links between sulfur, ethylene and polyamine biosynthesis. The Biochemical Journal **451**, 145–154.

Thomson CJ, Marschner H, Römheld V. 1993. Effect of nitrogen fertilizer form on pH of the bulk soil and rhizosphere, and on the growth, phosphorus, and micronutrient uptake of bean. Journal of Plant Nutrition **16**, 493–506.

Tyanova S, Temu T, Sinitcyn P, Carlson A, Hein MY, Geiger T, Mann M, Cox J. 2016. The Perseus computational platform for comprehensive analysis of (prote)omics data. Nature Methods **13**, 731–740.

Van Beusichem ML, Kirkby EA, Baas R. 1988. Influence of nitrate and ammonium nutrition on the uptake, assimilation, and distribution of nutrients in *Ricinus communis*. Plant Physiology **86**, 914–921.

Zhu CQ, Zhang JH, Zhu LF, *et al.* 2018. NH_4^+ facilitates iron reutilization in the cell walls of rice (*Oryza sativa*) roots under iron-deficiency conditions. Environmental and Experimental Botany **151**, 21–31.

Zhu CQ, Zhu XF, Hu AY, Wang C, Wang B, Dong XY, Shen RF. 2016. Differential effects of nitrogen forms on cell wall phosphorus remobilization are mediated by nitric oxide, pectin content, and phosphate transporter expression. Plant Physiology **171**, 1407–1417.

Zhu XF, Dong XY, Wu Q, Shen RF. 2019. Ammonium regulates Fe deficiency responses by enhancing nitric oxide signaling in *Arabidopsis thaliana*. Planta **250**, 1089–1102.

Zou C, Shen J, Zhang F, Guo S, Rengel Z, Tang C. 2001. Impact of nitrogen form on iron uptake and distribution in maize seedlings in solution culture. Plant and Soil **235**, 143–149.